Spectroscopic and Ligand-field Analysis of the Spin–Orbit Interaction between the ^1E_g and $^3T_{2g}$ States in Bis(1,4,7-triazacyclononane)nickel(II)†

Robert Stranger,* Steven C. Wallis, Lawrence R. Gahan, Colin H. L. Kennard and Karl A. Byriel
Department of Chemistry, The University of Queensland, QLD, 4072, Australia

The low-temperature single-crystal absorption spectrum, far-infrared spectrum and single-crystal structure determination of $[Ni(tacn)_2][ClO_4]_2 \cdot H_2O$ (tacn = 1,4,7-triazacyclononane) are reported. The compound crystallizes in the monoclinic space group $P2_1/a$ ($Z = 2$) with $a = 9.614(3)$, $b = 13.451(6)$, $c = 9.648(4)$ Å and $\beta = 120.11(1)°$. The $[Ni(tacn)_2]^{2+}$ complex ion is centrosymmetric, possessing approximate D_{3d} molecular symmetry. Trigonal splitting of the NiN_6 octahedral modes of vibration as well as several macrocyclic ring-deformation modes were observed in the far-infrared spectrum. From a detailed ligand-field analysis using the angular overlap model, the relative contributions of low-symmetry splitting and spin–orbit coupling within the $^3T_{2g}$ state *versus* spin–orbit mixing between the ^1E_g and $^3T_{2g}$ states were determined in relation to the anomalous double-humped $^3A_{2g} \longrightarrow {}^3T_{2g}$ band envelope. Although the trigonal-field splitting of both $^3T_{1g}$ states is large, it is quite small for the $^3T_{2g}$ state, consequently, the $^3A_{2g} \longrightarrow {}^3T_{2g}$ bandshape is shown to arise predominantly from spin–orbit mixing between the ^1E_g and $^3T_{2g}$ states even though the ^1E_g state contributes less than 10% to the overall band envelope. The double-humped bandshape feature is shown to be the result of two relatively narrow bands corresponding to transitions to spin–orbit levels which contain significant spin-singlet character. The best fit ligand-field parameters are $e_\sigma(N) = 4340$, $B = 840$, $C = 2830$ and $\zeta = 500$ cm^{-1}. The Racah parameters B and C are in good agreement with those found for other NiN_6 complexes.

The lowest-energy band, corresponding to the $^3A_{2g} \longrightarrow {}^3T_{2g}$ transition, of octahedral complexes of Ni^{II} containing nitrogen and sulfur donor ligands, often exhibits pronounced asymmetry giving rise to a characteristic double-humped bandshape.[1–7] The double-humped nature has been the subject of much controversy, being attributed to either low-symmetry splitting or spin–orbit splitting of the $^3T_{2g}$ state, or to the close approach of the ^1E_g state such that the spin-forbidden $^3A_{2g} \longrightarrow {}^1E_g$ transition gains appreciable intensity from the spin-allowed $^3A_{2g} \longrightarrow {}^3T_{2g}$ transition through spin–orbit coupling.[1,2,4,5,8] In the absence of unambiguous assignments for the $^3T_{2g}$ and ^1E_g states, the double-humped shape of the $^3A_{2g} \longrightarrow {}^3T_{2g}$ band has previously led to unrealistic values for the Racah B electron-repulsion parameter as well as erroneous values for $10Dq$.[2,4,5,9,10] Furthermore, the common assumption that the $^3A_{2g} \longrightarrow {}^1E_g$ and $^3A_{2g} \longrightarrow {}^3T_{2g}$ transitions may be of comparable intensity if considerable spin–orbit mixing occurs between the ^1E_g and $^3T_{2g}$ states is incorrect.[5,7] In fact, in the octahedral approximation, assuming that all $^3T_{2g}$ spin–orbit components contribute equally to the transition intensity, the maximum intensity that the ^1E_g state can borrow and therefore contribute to the $^3A_{2g} \longrightarrow {}^3T_{2g}$ band envelope is only 11%.

The lowest-energy band in the room-temperature solution spectrum of bis(1,4,7-triazacyclononane)nickel(II),[4,11] $[Ni(tacn)_2]^{2+}$, exhibits the characteristic double-humped bandshape typically observed for other complexes such as $[Ni(bipy)]^{2+}$ (bipy = 2,2′-bipyridine), $[Ni(en)_3]^{2+}$ (en = ethane-1,2-diamine), $[Ni(tasn)_2]^{2+}$ (tasn = 1-thia-4,7-diazacyclonone), $[Ni(daes)_2]^{2+}$ [daes = bis(2-aminoethyl) sulfide] and $[Ni(phen)_3]^{2+}$ (phen = 1,10-phenanthroline).[1–3,5] The ligand-field parameters $Dq = 1250$ cm^{-1} and $B = 993$ cm^{-1} were originally reported for $[Ni(tacn)_2]^{2+}$ on the basis of the solution data.[11] The unrealistically high value of B (*cf.* free-ion value of 1030 cm^{-1}) was attributed to trigonal-field-splitting effects. Later, the low-temperature mull spectrum of $[Ni(tacn)_2][ClO_4]_2$ was reported and analysed on the basis of a trigonally adapted, ligand-field model.[4] The low-energy shoulder observed for the $^3A_{2g} \longrightarrow {}^3T_{2g}$ transition was attributed to trigonal-field splitting and assigned to the ^3E_g trigonal component of the $^3T_{2g}$ state. However, the analysis only resulted in a slightly reduced B value of 980 cm^{-1}.

The single-crystal structure of $[Ni(tacn)_2](NO_3)Cl \cdot H_2O$ has been reported[12] and is consistent with a moderate trigonal distortion of the $[Ni(tacn)_2]^{2+}$ moiety. Clearly, since the trigonal distortion and spin–orbit coupling effects in this complex cannot be ignored in any spectral investigation, we now report a detailed low-temperature single-crystal absorption study and ligand-field analysis (using the angular overlap model) of $[Ni(tacn)_2][ClO_4]_2 \cdot H_2O$ in order to ascertain the relative importance of these effects on the observed $^3A_{2g} \longrightarrow {}^3T_{2g}$ bandshape. Although the crystal structure is known for $[Ni(tacn)_2](NO_3)Cl \cdot H_2O$, the perchlorate salt was more suitable for study as the nitrate ion exhibits an internal transition which partly obscures the $^3A_{2g} \longrightarrow {}^3T_{1g}(P)$ transition in the near-UV region. In order to compare the geometries of the $[Ni(tacn)_2]^{2+}$ chromophores in the two salts, and to provide a framework for ligand-field analysis, we also report the single-crystal structure determination of $[Ni(tacn)_2][ClO_4]_2 \cdot H_2O$.

Experimental

Preparation.—The compound $[Ni(tacn)_2][ClO_4]_2 \cdot H_2O$ was prepared as previously described[11] and recrystallized from aqueous solution. Pink crystals of suitable size for X-ray diffraction and spectroscopy were grown by slow evaporation from aqueous solution. Isolated crystals are sensitive to solvent loss and dehydrate appreciably after a few hours in the open air.

Structure Determination.—All X-ray data were collected on a Enraf-Nonius CAD-4 diffractometer using graphite-mono-

---

† *Supplementary data available:* see Instructions for Authors, *J. Chem. Soc., Dalton Trans.*, 1992, Issue 1, pp. xx–xxv.

Table 1 Crystallographic data for $[Ni(tacn)_2]_2[ClO_4]_2{\cdot}H_2O$

M	516.01
Crystal system	Monoclinic
Space group	$P2_1/a$
a/Å	9.614(3)
b/Å	13.451(6)
c/Å	9.648(4)
β/°	120.110(14)
U/Å^3	1079.3(8)
D_c/g cm^{-3}	1.637
Z	2
Crystal size/mm	0.08 × 0.20 × 0.36
μ(Mo-Kα)/cm^{-1}	12.1
T/K	298
Scan type	ω
Scan width/°	0.7
Scan speed/° min^{-1}	0.84
Data collection range, 2θ/°	2–50
No. measured reflections; $I_o > 2.5\sigma(I)$	2172
No. independent reflections	1446
$F(000)$	556
w	$1/[\sigma^2(F_o) + 0.000\,209F_o^2]$
R	0.027
R'	0.029

Table 2 Non-hydrogen positional parameters for $[Ni(tacn)_2][ClO_4]_2{\cdot}H_2O$

Atom	X/a	Y/b	Z/c
Ni	1.000 0	0.000 0	1.000 0
Cl(1)	0.407 64(8)	0.131 70(5)	0.793 43(9)
N(1)	0.970 6(3)	0.066 9(2)	0.788 5(3)
C(2)	0.797 8(4)	0.091 8(2)	0.693 8(3)
C(3)	0.697 1(3)	0.003 0(2)	0.682 7(3)
N(4)	0.762 9(2)	−0.047 1(2)	0.841 0(3)
C(5)	0.771 8(3)	−0.156 0(2)	0.832 0(3)
C(6)	0.907 3(3)	−0.186 2(2)	0.803 3(3)
N(7)	1.053 8(3)	−0.126 4(2)	0.902 9(2)
C(8)	1.127 2(3)	−0.084 7(2)	0.812 9(3)
C(9)	1.022 3(3)	−0.002 3(2)	0.702 4(3)
O(1)	0.553 9(3)	0.186 1(2)	0.849 8(3)
O(2)	0.304 0(3)	0.153 6(2)	0.629 9(3)
O(3)	0.331 4(3)	0.160 5(2)	0.882 0(3)
O(4)	0.439 8(3)	0.028 3(2)	0.810 7(4)
O(w1)	0.488 1(8)	0.267 9(5)	0.513 5(6)

Table 3 Selected bond lengths (Å) and angles (°) in $[Ni(tacn)_2][ClO_4]_2{\cdot}H_2O$

Ni–N(1)	2.115(3)	Ni–N(4)	2.108(3)
Ni–N(7)	2.126(2)	O(1)–Cl(1)	1.429(3)
O(2)–Cl(1)	1.411(3)	O(3)–Cl(1)	1.430(3)
O(4)–Cl(1)	1.416(3)	N(1)–C(2)	1.478(5)
N(1)–C(9)	1.489(4)	N(4)–C(3)	1.489(4)
N(4)–C(5)	1.473(4)	N(7)–C(6)	1.482(4)
N(7)–C(8)	1.477(4)	C(2)–C(3)	1.507(4)
C(5)–C(6)	1.517(5)	C(8)–C(9)	1.518(4)
N(1)–Ni–N(4)	81.57(10)	N(1)–Ni–N(7)	81.92(8)
N(4)–Ni–N(7)	81.52(10)	N(1)–Ni–N(4′)	98.43(10)
N(1)–Ni–N(7′)	98.07(8)	N(4)–Ni–N(7′)	98.50(10)
O(1)–Cl(1)–O(2)	109.07(17)	O(1)–Cl(1)–O(3)	109.58(16)
O(2)–Cl(1)–O(3)	108.98(18)	O(1)–Cl(1)–O(4)	110.07(18)
O(2)–Cl(1)–O(4)	109.06(18)	O(3)–Cl(1)–O(4)	110.05(18)
Ni–N(1)–C(2)	104.9(2)	Ni–N(1)–C(9)	110.58(15)
Ni–N(4)–C(3)	111.02(17)	Ni–N(4)–C(5)	105.55(17)
Ni–N(7)–C(6)	110.9(2)	Ni–N(7)–C(8)	104.44(15)
C(2)–N(1)–C(9)	112.5(2)	C(3)–N(4)–C(5)	113.4(2)
C(6)–N(7)–C(8)	113.81(19)	N(1)–C(2)–C(3)	110.3(2)
N(1)–C(9)–C(8)	110.8(2)	N(4)–C(3)–C(2)	111.0(2)
N(4)–C(5)–C(6)	110.9(2)	N(7)–C(6)–C(5)	111.1(2)
N(7)–C(8)–C(9)	110.2(3)		

chromatized Mo-Kα radiation ($\lambda = 0.710\,69$ Å). Initial cell dimensions were obtained from the angle data for 25 independent reflections between 2θ 24 and 26°. Lorentz, polarization and absorption corrections were applied using the CAD-4 SDP packages.[13] Neutral atom scattering factors and anomalous dispersion corrections for nickel were taken from ref. 14, while for all other atoms the values supplied in SHELX 76[15] were used. The structure was solved by Patterson techniques using SHELX 86[16] and refined by full-matrix least-squares methods using SHELX 76. Hydrogen atoms were located from a Fourier difference map and were included in the refinement with isotropic thermal parameters in the last stages. Thermal parameters for all non-hydrogen atoms were refined anisotropically. Final refinement using 1446 observed reflections yielded an R' factor of 0.029. The crystallographic data are given in Table 1, the final non-hydrogen atomic coordinates in Table 2, and selected interatomic bond lengths and angles in Table 3.

Additional material available from the Cambridge Crystallographic Data Centre comprises H-atom coordinates, thermal parameters and remaining bond lengths and angles.

Spectroscopy and Ligand-field Analysis.—Absorption spectra were measured on a Cary 17 spectrophotometer interfaced to a personal computer to allow data acquisition and control of the instrument. The original detectors were replaced with more sensitive components, namely a Hamamatsu R636 GaAs photomultiplier tube for the UV–VIS region and a P2682 thermoelectrically cooled PbS photoconductive cell and C1103-02 temperature controller for the near-IR region. Single crystals were mounted over a hole in a copper plate with rubber cement adhesive. Low-temperature spectra (down to 10 K) were obtained using a Leybold-Heraeus ROK 10-300 closed-cycle helium cryostat system. Owing to significant dehydration of the crystals under vacuum it was necessary to cool the sample to *ca.* 250 K under atmospheric conditions before evacuating the cryostat and cooling further. A background spectrum was recorded under identical conditions by removing the crystal from the copper plate.

Far-infrared spectra at room temperature and 4 cm^{-1} resolution were recorded using a Digilab FTS 20E Fourier-transform infrared spectrometer on Nujol mulls between Polythene plates. Spectral manipulation and presentation, including band analysis, were performed using the software package SpectraCalc by Galactic Industries. Ligand-field calculations were carried out in the framework of the angular overlap model (AOM) using the computer program CAMMAG.[17]

Results and Discussion

Crystal Structure.—The relevant single-crystal structure data for $[Ni(tacn)_2][ClO_4]_2{\cdot}H_2O$ are reported in Tables 1–3. The structure with relevant atoms labelled, is shown in Fig. 1. It comprises the near-octahedral $[Ni(tacn)_2]^{2+}$ complex ion, two perchlorate anions and half a water molecule (one per unit cell). There is hydrogen bonding between the hydrogen of the amine groups and the oxygen of the perchlorate molecules. The $[Ni(tacn)_2]^{2+}$ ion is centrosymmetric, occupying a site of C_i symmetry, but approximates D_{3d} molecular symmetry analogous to that reported for $[Ni(tacn)_2](NO_3)Cl$.[12] In both structures the trigonal distortion is predominantly due to an elongation along the pseudo-C_3 axis with very similar average polar angles θ (angle between a Ni–N bond vector and the C_3 axis) of 49.0(2) and 49.6(3)° for $[Ni(tacn)_2][ClO_4]_2{\cdot}H_2O$ and $[Ni(tacn)_2](NO_3)Cl$, respectively, in relation to 54.75° for a regular octahedron. The average trigonal twist angles φ (angle between the upper and lower trigonally displaced sets of ligands) however differ between the two stuctures. In

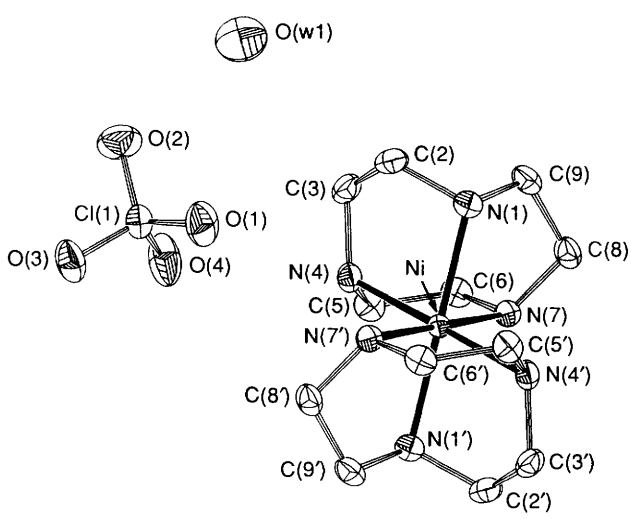

Fig. 1 Structure of $[Ni(tacn)_2][ClO_4]_2{\cdot}H_2O$ with relevant atoms labelled. Hydrogen atoms are not shown

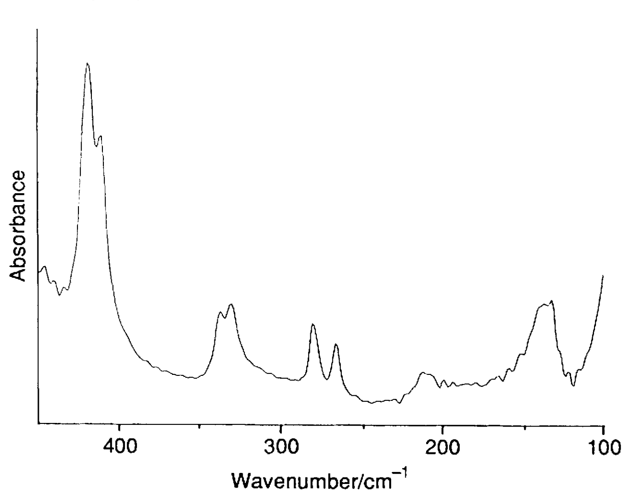

Fig. 2 Far-infrared absorption spectrum of $[Ni(tacn)_2][ClO_4]_2{\cdot}H_2O$

$[Ni(tacn)_2](NO_3)Cl$ (φ = 56.2(8)° whereas for $[Ni(tacn)_2][ClO_4]_2{\cdot}H_2O$ the average twist angle of 60.0(3)° is exactly the octahedral value. The average Ni–N bond length of 2.116(9) Å for $[Ni(tacn)_2][ClO_4]_2{\cdot}H_2O$ is comparable to that of 2.105(12) Å for $[Ni(tacn)_2](NO_3)Cl$. The intra- and inter-ring N–Ni–N bond angles average 81.6(3) and 98.4(1)° compared to 82.6(18) and 97.5(18)° for $[Ni(tacn)_2](NO_3)Cl$.

Infrared Spectrum.—The far-infrared absorption spectrum from 450 to 100 cm^{-1} is shown in Fig. 2. For $[Ni(tacn)_2]^{2+}$ there are 51 normal modes of vibration (excluding rotation and translation modes as well as vibrations involving hydrogen atoms) spanning $5A_{1g} + 3A_{2g} + 8E_g + 4A_{1u} + 5A_{2u} + 9E_u$ irreducible representations in D_{3d} symmetry. For descriptive purposes the vibrations can be classified as ν(MN) $A_{1g} + E_g + A_{2u} + E_u$, ν(NC) $A_{1g} + A_{2g} + 2E_g + A_{1u} + A_{2u} + 2E_u$, ν(CC) $A_{1g} + E_g + A_{2u} + E_u$, δ(NMN) $A_{1g} + E_g + A_{1u} + A_{2u} + 2E_u$ and δ(ring) $A_{1g} + 2A_{2g} + 3E_g + 2A_{1u} + A_{2u} + 3E_u$, where the A_{2u} and E_u modes are infrared active.

For an octahedral NiN_6 entity the normal modes of vibration span $A_{1g} + E_g + T_{2g} + 2T_{1u} + T_{2u}$ irreducible representations. In the octahedral limit, only two of these species are infrared active, corresponding to the antisymmetric Ni–N stretch and N–Ni–N deformation modes of T_{1u} symmetry. For D_{3d} symmetry, the T_{1u} modes split into $A_{2u} + E_u$ components, both of which are infrared active. Furthermore, the E_u trigonal component of the previously inactive T_{2u} mode may also be observed. Of the macrocyclic ring modes, the C–C and N–C stretching vibrations should occur around 1000 cm^{-1} as is the case for $[M(en)_3]^{2+}$ complexes.[18,19] The macrocyclic ring deformation modes can be grouped into N–C–C or Ni–N–C deformation modes, some of which will also involve torsional motion of the ring.[20,21] For $[Ni(en)_3]^{2+}$, ring deformation modes were observed at approximately 530, 500 and 230 cm^{-1}.[19] In addition, the band reported at around 130 cm^{-1} should also be assigned to a ring-deformation mode (involving mainly torsional motion around the Ni–N bond) on the basis of normal coordinate calculations for $[Co(en)_3]^{3+}$.[20,21] Hence, below 600 cm^{-1}, nine infrared-active vibrational species (five NiN_6 skeletal modes and four macrocyclic ring-deformation modes) are possible.

In the absence of normal coordinate calculations for $M(tacn)_2$ complexes, the vibrational assignments and normal coordinate calculations for $M(en)_3$ complexes[19–21] serve as a guideline for assignments. The split band with peaks at 421 and 412 cm^{-1} (Fig. 2) is assigned to the trigonal components of the T_{1u} antisymmetric stretch mode on the basis that the same vibration is observed at *ca.* 410 cm^{-1} for $[Ni(en)_3]^{2+}$.[18,19] Similarly, the weak split band with peaks at 338 and 332 cm^{-1} is assigned to the trigonal components of the antisymmetric T_{1u} deformation as this mode is observed at *ca.* 329 cm^{-1} for $[Ni(en)_3]^{2+}$. The weak sharp bands at 280 and 266 cm^{-1} are assigned to macrocyclic ring-deformation modes as a chelate ring-deformation mode was observed at *ca.* 230 cm^{-1} for $[Ni(en)_3]^{2+}$. The broad, moderately intense band at *ca.* 138 cm^{-1} is also assigned to a low-energy macrocyclic ring-deformation mode involving mainly Ni–N torsional motion. The weak broad band observed at *ca.* 212 cm^{-1} is tentatively assigned to the E_u trigonal component of the T_{2u} deformation mode as normal coordinate calculations for $[M(en)_3]^{3+}$ complexes indicate that this mode should occur at around 200 cm^{-1}.[20,21]

Electronic Spectroscopy.—The single-crystal absorption spectra of $[Ni(tacn)_2][ClO_4]_2{\cdot}H_2O$ at approximately 10 and 250 K are shown in Fig. 3. Broad bands centred at approximately 12 500, 19 700 and 30 850 cm^{-1} are straightforwardly assigned to the $^3A_{2g} \longrightarrow {}^3T_{2g}$, $^3A_{2g} \longrightarrow {}^3T_{1g}(F)$ and $^3A_{2g} \longrightarrow {}^3T_{1g}(P)$ spin-allowed transitions of d^8 octahedral parentage. The weak, sharp feature observed at *ca.* 20 900 cm^{-1} on the high-energy side of the $^3A_{2g} \longrightarrow {}^3T_{1g}(F)$ transition has not been previously observed and is assigned to the $^3A_{2g} \longrightarrow {}^1A_{1g}$ spin-forbidden transition on the basis that the same transition occurs between 20 900 and 22 500 cm^{-1} in the low-temperature spectra of other $NiN_6{}^{2+}$ complexes.[2,3,22] The observation of this transition is important as it allows the unique determination of the octahedral ligand-field parameters *B*, *C* and *Dq* from which an initial prediction of the position of the spin-forbidden $^3A_{2g} \longrightarrow {}^1E_g$ transition is possible. The low-energy shoulders observed at approximately 17 900 and 11 600 cm^{-1} in the spectrum at 10 K have previously been assigned to the ^3E_g components of the trigonally split $^3T_{1g}(F)$ and $^3T_{2g}$ states, respectively.[4] The sharp band structure observed in both the spectra at 10 and 250 K between 4000 and 10 000 cm^{-1} is assigned to vibrational combination bands.

For D_{3d} symmetry, all d–d transitions are statically forbidden by an electric-dipole process, but may acquire intensity through either a magnetic-dipole mechanism or vibronic coupling. Some measure of the vibronically induced electric-dipole character of the spectrum may be gained from a temperature-dependence study. Unfortunately, due to crystal dehydration effects under vacuum, it was only possible to measure the crystal absorption spectra at 10 and 250 K. However, a comparison of the spectra at 10 and 250 K shown in Fig. 3 reveals that a vibronic electric-dipole mechanism is operative as the higher-temperature spectrum has increased in intensity between 30 and 50% for the three spin-allowed transitions. For D_{3d} symmetry, transitions from the $^3A_{2g}$ ground state to all trigonal components of the $^3T_{2g}$ and $^3T_{1g}$ states are allowed by a

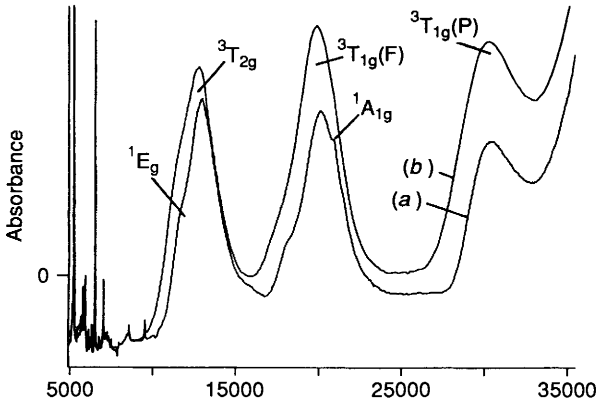

Fig. 3 Single-crystal absorption spectra of $[Ni(tacn)_2][ClO_4]_2{\cdot}H_2O$ at 10 (*a*) and 250 K (*b*)

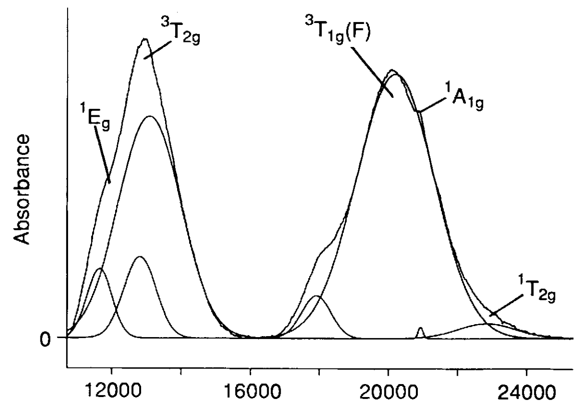

Fig. 4 Band analysis of the $^3A_{2g} \longrightarrow {}^3T_{2g}$ and $^3A_{2g} \longrightarrow {}^3T_{1g}(F)$ transitions in the absorption spectrum of $[Ni(tacn)_2][ClO_4]_2{\cdot}H_2O$ at 10 K

vibronic electric-dipole mechanism and therefore without polarization data it is not possible to discriminate futher.

Both the $^3T_{2g}$ and $^3T_{1g}(F)$ band envelopes in the crystal spectrum at 10 K were subjected to deconvolution and subsequent gaussian analysis to locate the underlying components. In the case of the $^3T_{2g}$ band the analysis was initially constrained to a maximum of three gaussian curves corresponding to the two trigonal components of the $^3T_{2g}$ state and a single component for the ^1E_g state. The $^3T_{1g}(F)$ band analysis was constrained to a maximum of four gaussian curves corresponding to the two trigonal components of the $^3T_{1g}(F)$ state and single components for each of the ^1A_g and $^1T_{2g}$ states. The results of the band analysis are shown in Fig. 4 where good fits are obtained with three and four gaussian components respectively, for the $^3T_{2g}$ and $^3T_{1g}(F)$ band envelopes. From the analysis, the position of the weak spin-forbidden $^3A_{2g} \longrightarrow {}^1T_{2g}$ transition is located at approximately 23 000 cm^{-1} but due to baseline problems its position cannot be relied upon with any certainty.

Ligand-field Analysis.—In order to obtain initial estimates of the ligand-field parameters, the broad band centres observed at approximately 12 500, 19 700 and 30 850 cm^{-1} in the room-temperature solution spectrum, as well as the weak spin-forbidden transition at *ca.* 20 900 cm^{-1} in the single-crystal spectrum at 10 K, were fitted using the full octahedral d^8 matrices to derive values of *B*, *C* and *Dq*. The best-fit values obtained were $B = 865$, $C = 2645$ and $Dq = 1250$ cm^{-1} and the observed *versus* calculated energies are given in Table 4.

Table 4 Observed and calculated octahedral energies for the room-temperature solution spectrum of $[Ni(tacn)_2]^{2+}$

Assignment		Energies (cm^{-1})		
State	Spin–orbit level	Observed	Calc. ($\zeta = 0$)	Calc. ($\zeta = 500$)
$^3T_{2g}$	T_1	12 500	12 500	12 390
	T_2			12 665
	E			12 700
	A_2			12 800
^1E_g	E	11 300	11 855	11 485
$^3T_{1g}(F)$	A_1	19 700	19 530	18 935
	T_1			19 375
	T_2			19 805
	E			19 880
$^1A_{1g}$	A_1	20 900*	20 900	21 140
$^1T_{2g}$	T_2		24 060	24 040
$^1T_{1g}$	T_1		28 150	28 205
$^3T_{1g}(P)$	E	30 850	30 915	30 900
	T_2			30 960
	T_1			31 075
	A_1			31 120

Parameters: $B = 865$, $C = 2645$, $Dq = 1250$ cm^{-1}

* $^3A_{2g} \longrightarrow {}^1A_{1g}$ transition not observed in solution spectrum, position taken from single-crystal spectrum at 10 K.

On the basis of these parameters, the $^3A_{2g} \longrightarrow {}^1E_g$ spin-forbidden transition is calculated to lie under the $^3T_{2g}$ band envelope at approximately 11 850 cm^{-1}, and therefore may be associated with the low-energy shoulder observed at *ca.* 11 500 cm^{-1}.

An additional calculation was undertaken in which the one-electron spin–orbit coupling parameter ζ was set to 500 cm^{-1} with the remaining ligand-field parameters fixed at the values given above. The results of this calculation are also given in Table 4. The value of $\zeta = 500$ cm^{-1} is reasonable on the basis that the parameter *B* has been reduced by approximately 20% from the free-ion value of 1030 cm^{-1}. Other workers have used ζ values between 400 and 500 cm^{-1}.[22] In the octahedral limit, the $^3T_{2g}$ state comprises $A_2 + E + T_1 + T_2$ spin–orbit levels while the ^1E_g state consists of just one spin–orbit level of E symmetry. Since the spin–orbit coupling operator is symmetry invariant, the spin-forbidden ^1E_g state can only mix with the E spin–orbit component of the $^3T_{2g}$ state, a point which has been overlooked by a number of workers.[5,7] The calculation reveals that, due to the close approach of the spin-forbidden ^1E_g state and the E spin–orbit level of the $^3T_{2g}$ state, considerable interaction occurs between these two levels with the ^1E_g state (defined as the level containing the most spin-singlet character) lying to lower energy at approximately 11 480 cm^{-1}, in very good agreement with the observed low-energy shoulder at around 11 500 cm^{-1}.

The above calculations ignore the trigonal-field and other low-symmetry splitting of the octahedral states which, on the basis of the observed splitting of the $^3T_{1g}(F)$ state in the single-crystal spectrum at 10 K, is not insignificant. To account for the low-symmetry splitting of the parent octahedral states, the angular overlap model was used where the low-symmetry potential was generated using the atomic coordinates of the nitrogen donor atoms obtained from the single-crystal structure determination. Since the ligating atoms are all pure σ-donor atoms towards Ni^{II}, only one AOM parameter, $e_\sigma(N)$, is required to model the ligand-field potential. The differences in Ni–N bond lengths can be accommodated by introducing a r^{-5} dependence of $e_\sigma(N)$ on bond length.[23,24]

To obtain a measure of the low-symmetry splitting of the octahedral states in the absence of spin–orbit coupling effects,

Table 5 Observed and calculated (AOM) energies for the low-temperature crystal spectrum of $[Ni(tacn)_2][ClO_4]_2\cdot H_2O$

Assignment		Energies (cm^{-1})*		
O_h	D_{3d}	Observed	Calc. ($\zeta = 0$)	Calc. ($\zeta = 500$)
$^3A_{2g}$	$^3A_{2g}$		0	0 3
^1E_g	^1E_g	11 630	12 020	11 590
$^3T_{2g}$	^3E_g	12 810	12 390	12 300 12 460 12 590 12 620 12 810 12 815
	$^3A_{1g}$	13 080	12 660	
$^3T_{1g}(F)$	$^3A_{2g}$	17 870	18 175	18 100 18 260 19 815 19 925 20 180 20 360
	^3E_g	20 100	20 075	
$^1A_{1g}$	$^1A_{1g}$	20 900	20 870	21 130
$^1T_{2g}$	^1E_g		23 965	23 940 24 965
	$^1A_{1g}$		24 980	
$^1T_{1g}$	^1E_g		28 080	28 140 28 450
	$^1A_{2g}$		28 410	
$^3T_{1g}(P)$	^3E_g	30 050	29 770	29 805 29 830 29 875 29 920 32 490 32 495
	$^3A_{2g}$		32 410	

Parameters: $B = 840$, $C = 2830$, $e_\sigma(N) = 4340\ cm^{-1}$

* Calculated energies for approximate D_{3d} symmetry.

AOM calculations were performed using the initial ligand-field parameter values for B and C determined from the above octahedral calculations and with $e_\sigma(N)$ set initially to $10Dq/3$. The parameter values were then adjusted to give the best fit to the observed positions of the $^3T_{2g}$, $^3T_{1g}(F)$, $^3T_{1g}(P)$ and $^1A_{1g}$ states. The resulting energy levels and best-fit ligand-field parameters are detailed in Table 5 on the basis of approximate D_{3d} symmetry.

Of particular significance is the large difference in the calculated low-symmetry splitting of the $^3T_{2g}$ state in relation to both $^3T_{1g}$ states. The pseudo-trigonal-field splitting of the $^3T_{2g}$ state is quite small, approximately 250 cm^{-1}, whereas the splitting of the $^3T_{1g}(F)$ and $^3T_{1g}(P)$ states is an order of magnitude larger, around 2500 cm^{-1}. Clearly, the low-energy shoulder at approximately 17 900 cm^{-1} can be assigned to the trigonal $^3A_{2g}$ component of the $^3T_{1g}(F)$ state. This is the reverse assignment to that reported by Alper and Zompa[4] on the basis of their ligand-field calculations using a trigonally adapted, ligand-field model. However, their values for the trigonal ligand-field parameters v and v′ are inconsistent with the known trigonal distortion in $[Ni(tacn)_2]^{2+}$.

The small splitting of the $^3T_{2g}$ state calculated using the angular overlap model, with the non-degenerate $^3A_{1g}$ trigonal component lying to higher energy, is in accordance with the small trigonal twist and trigonally elongated geometry observed for this complex. Alper and Zompa calculated a much larger trigonal splitting (*ca.* 1000 cm^{-1}) of the $^3T_{2g}$ state and on this basis assigned the low-energy shoulder on the $^3T_{2g}$ band envelope to the ^3E_g trigonal component rather than to the spin-forbidden $^3A_{2g} \longrightarrow {}^1E_g$ transition.

In order to investigate the extent of interaction between the ^1E_g and $^3T_{2g}$ states, an AOM calculation was undertaken in which spin–orbit coupling was included by setting ζ to 500 cm^{-1}. All other parameters were fixed at the above best-fit values of $B = 840$, $C = 2830$ and $e_\sigma(N) = 4340\ cm^{-1}$. The resulting energy levels are listed in Table 5 on the basis of approximate D_{3d} symmetry. The agreement between observed and calculated band positions is very good. Clearly, the low-energy shoulder on the $^3T_{2g}$ band envelope at 11 600 cm^{-1} in the spectrum at 10 K must be assigned to the spin-forbidden ^1E_g state and not to low-symmetry splitting of the $^3T_{2g}$ state as previously proposed.[4] From the calculation, the spin-forbidden ^1E_g state mixes extensively with several of the $^3T_{2g}$ spin–orbit levels calculated between 12 600 and 12 850 cm^{-1}. The Racah B value is now much more acceptable than the previously reported value of 980 cm^{-1}, and is close to B values of 880 and 885 cm^{-1} calculated for $[Ni(NH_3)_6]^{2+}$ and $[Ni(en)_3]^{2+}$ on the basis of the band positions reported in the low-temperature spectra of these two complexes.[3,22] The Racah C parameter is also in good agreement with values of 3300 and 2870 cm^{-1} determined for these two complexes. The $e_\sigma(N)$ value is close to the octahedral value of $10Dq/3$ for pure σ-donor ligands.

Since the trigonal-field splitting of the $^3T_{2g}$ state is relatively small, an additional calculation was carried out in the octahedral limit to determine the approximate degree of mixing between the $^3T_{2g}$ and ^1E_g states. In this calculation Dq was adjusted slightly to give the best fit to the observed band positions for the $^3T_{2g}$ and ^1E_g states. The remaining ligand-field parameters were unchanged from those given above. The calculated energies for the ^1E_g state and T_1, T_2, E and A_2 spin–orbit levels of the $^3T_{2g}$ state were 11 625, 12 390, 12 665, 12 770 and 12 800 cm^{-1}, respectively. The separation of the ^1E_g and $^3T_{2g}(E_g)$ levels is close to the minimum separation of approximately 1100 cm^{-1} calculated in the octahedral approximation with $\zeta = 500\ cm^{-1}$. As a consequence, the ^1E_g state and the E spin–orbit level of the $^3T_{2g}$ state are extensively mixed, comprising approximately 40 and 60% spin-triplet character, respectively.

In the absence of spin–orbit coupling, the $^3A_{2g} \longrightarrow {}^1E_g$ spin-forbidden transition is quite sharp but will broaden and increase in intensity as a function of the spin-triplet character mixed into the ^1E_g state through spin–orbit interaction with the $^3T_{2g}$ state. Conversely, the $^3A_{2g} \longrightarrow {}^3T_{2g}$ transition is broad but the transition to the E spin–orbit level of the $^3T_{2g}$ state will sharpen and decrease in intensity with increasing spin-singlet character mixed-in through spin–orbit interaction with the ^1E_g state. Since the two weak gaussian components at approximately 11 600 and 12 800 cm^{-1} (Fig. 4) are quite narrow in relation to the major gaussian component at around 13 000 cm^{-1}, they are accordingly assigned to the ^1E_g state and E spin–orbit level of the $^3T_{2g}$ state respectively, due to the substantial spin-singlet character associated with these two states. Their separation of *ca.* 1200 cm^{-1} is very close to the calculated minimum separation of *ca.* 1100 cm^{-1} where equal mixing between the two levels is expected, and this is consistent with the observed similarity in bandshape and intensity. The calculated position of the E spin–orbit level of the $^3T_{2g}$ state corresponds closely to the observed $^3T_{2g}$ band maxima around 12 800 cm^{-1}, hence the spin-singlet character (*ca.* 40%) mixed into this formally $^3T_{2g}$ spin–orbit level accounts for the observed sharpness of the $^3T_{2g}$ band maxima in relation to the higher-lying $^3T_{1g}$ band envelopes.

Although the mixing between the formally octahedral ^1E_g state and the E_g spin–orbit level of the $^3T_{2g}$ state is significant, the spin-forbidden $^3A_{2g} \longrightarrow {}^1E_g$ transition only accounts for at most 10% of the total intensity of the $^3T_{2g}$ band envelope. In this respect, the double-humped $^3T_{2g}$ bandshape observed for $[Ni(tacn)_2]^{2+}$ is not so much attributable to an appreciable gain in intensity of the spin-forbidden $^3A_{2g} \longrightarrow {}^1E_g$ transition through spin–orbit coupling with the $^3T_{2g}$ state, but to the product of the narrow bandwidths resulting for transitions to the spin–orbit levels containing significant spin-singlet character. Considering the similarity in absorption spectra, the same conclusion is likely to apply to the double-humped

$^3A_{2g} \longrightarrow {}^3T_{2g}$ band envelope observed for the trigonal complexes $[Ni(bipy)_3]^{2+}$, $[Ni(phen)_3]^{2+}$ and $[Ni(en)_3]^{2+}$.[1,3]

From the above spectral analysis of $[Ni(tacn)_2]^{2+}$ it is clear that the double-humped bandshape observed for the $^3A_{2g} \longrightarrow {}^3T_{2g}$ transition of other octahedral nickel(II) complexes cannot in all cases be simply attributed to a significant intensity enhancement of the spin-forbidden $^3A_{2g} \longrightarrow {}^1E_g$ transition through spin–orbit mixing with the $^3T_{2g}$ state. Indeed, as seen in the present analysis, with the observation of the $^3A_{2g} \longrightarrow {}^1A_{1g}$ spin-forbidden transition, the position of the ^1E_g state cannot be ascertained with any reliability. Each complex must be analysed on its own merit since the contributions of low-symmetry splitting and spin–orbit coupling effects will differ in each case. For example, the double-humped bandshape observed for the $^3A_{2g} \longrightarrow {}^3T_{2g}$ transition in $[Ni(tasn)_2]^{2+}$,[5] containing the *trans* $Ni(N_4S_2)^{2+}$ isomer, may well be the result of low-symmetry splitting effects rather than spin–orbit mixing between the ^1E_g and $^3T_{2g}$ states.

Acknowledgements

We acknowledge the use of facilities at the Central Science Laboratory, University of Tasmania, in order to measure far-infrared spectra.

References

1 C. K. Jørgensen, *Acta Chem. Scand.*, 1955, **9**, 1362.
2 R. A. Palmer and T. S. Piper, *Inorg. Chem.*, 1966, **5**, 864.
3 R. Dingle and R. A. Palmer, *Theor. Chim. Acta*, 1966, **6**, 249.
4 J. S. Alper and L. J. Zompa, *Inorg. Nucl. Chem.*, 1980, **42**, 1693.
5 S. M. Hart, J. C. A. Boeyans and R. D. Hancock, *Inorg. Chem.*, 1983, **22**, 982.
6 L. R. Gahan and T. W. Hambley, *Transition Met. Chem.*, 1988, **13**, 72.
7 M. A. Robinson, J. D. Curry and D. H. Busch, *Inorg. Chem.*, 1963, **2**, 1178.
8 A. D. Liehr and C. J. Ballhausen, *Ann. Phys. (N.Y.)*, 1959, **6**, 134.
9 L. J. Zompa, *Inorg. Chem.*, 1978, **17**, 2531.
10 E. B. Fleischer, A. E. Gebala, D. R. Swift and P. A. Tasker, *Inorg. Chem.*, 1972, **11**, 2775.
11 R. Yang and L. J. Zompa, *Inorg. Chem.*, 1976, **15**, 1499.
12 L. J. Zompa and T. N. Margulis, *Inorg. Chim. Acta*, 1978, **28**, L157.
13 Enraf-Nonius Structure Determination Package, Enraf-Nonius, Delft, 1985.
14 J. A. Ibers and W. C. Hamilton (Editors), *International Tables for X-Ray Crystallography*, Kynoch Press, Birmingham, 1974, vol. 4.
15 G. M. Sheldrick, SHELX 76, Program for X-Ray Crystal Structure Determinations, University of Cambridge, 1976.
16 G. M. Sheldrick, SHELXS 86, Program for Solution of Crystal Structures, University of Gottingen, 1986.
17 D. A. Cruse, J. E. Davies, M. Gerloch, J. H. Harding, D. J. Mackey and R. F. McMeeking, CAMMAG, a Fortran Computing Package, University Chemical Laboratory, Cambridge, 1979.
18 D. B. Powell and N. Sheppard, *Spectrochim. Acta*, 1961, **17**, 68.
19 Z. Gabelica, *Spectrochim. Acta, Part A*, 1976, **32**, 327.
20 G. Borch, P. H. Nielsen and P. Klæboe, *Acta Chem. Scand., Ser. A*, 1977, **31**, 109.
21 B. E. Williamson, L. Dubicki and S. E. Harnung, *Inorg. Chem.*, 1988, **27**, 3484.
22 A. F. Schreiner and D. J. Ham, *Inorg. Chem.*, 1973, **12**, 2037.
23 S. Minomura and H. G. Drickamer, *J. Chem. Phys.*, 1961, **35**, 903.
24 D. W. Smith, *J. Chem. Phys.*, 1969, **50**, 2784.

Received 10*th March* 1992; *Paper* 2/01298G